Author's Response to Reviewers' Comments

Manuscript: essd-2025-583

Global Surface Mining and Land Reclamation Time Series from 1985–2022

Dear Editor and Reviewers,

We sincerely thank the referees for their careful reading of our manuscript and for their constructive comments. These comments helped us clarify the methodological scope of the dataset, particularly its dependence on GLC_FCS30D, the temporal constraints of the source land-cover product, and the distinction between boundary refinement, land-cover-transition inference, temporal validation, and recent status classification. In the revised manuscript, we have clarified that DEV and REC are inferred from land-cover transitions within known mining boundaries rather than from direct spectral-temporal breakpoint detection, added a cross-product sensitivity assessment using CLCD, expanded the discussion of uncertainty propagation and temporal limitations, and revised several figures and captions for consistency and accessibility. Below we provide a consolidated point-by-point response to all comments. Our replies are shown in blue text. Line numbers refer to the revised manuscript.

Response to Report #1 - Anonymous referee #1

Comment 1: Indirect disturbance inference

Reviewer's Comment: *"Mining disturbance and reclamation are not directly derived from satellite spectral–temporal change detection, but inferred from the GLC_FCS30D land use and land cover time-series product combined with rule-based indices. The framework is therefore structurally dependent on a general-purpose LULC dataset rather than direct spectral change retrieval."*

Response:

We thank the referee for this important methodological clarification, and we agree. Our DEV and REC layers are not direct spectral–temporal breakpoint products; they are inferred from GLC_FCS30D land-cover transitions within pre-defined mining boundaries. Several openly available global LULC products exist (Table R1), but only GLC_FCS30D combines the spatial and temporal resolution required for this study. Other products are limited by coarser resolution, short or single-year coverage, or discrete epochs. Direct spectral-breakpoint methods (e.g., LandTrendr, CCDC) can in principle retrieve disturbance events directly from Landsat reflectance, but parameter tuning of breakpoint method and noise in Landsat image collection (e.g., Landsat-7 SLC-off issue, cross-sensor harmonization) pose greater uncertainty at the global scale they require harmonized multi-sensor reflectance, careful cloud and SLC-off handling, and consistent class-attribution rules; running such a workflow globally over 1985–2022 was beyond the practical scope of this study. We have revised the Methods so that this dependence is explicit, and we now consistently refer to DEV/REC as "GLC_FCS30D-based land-cover transition layers" rather than as direct spectral-change products. We have also clarified that "reclamation" in this dataset refers to remotely sensed greening or revegetation signals, not field-confirmed ecological restoration.

Table R1 Openly available global LULC products considered for this study.

Product	Resolution	Temporal coverage	Time step	Source
GLC_FCS30D	**30 m**	**1985–2022**	**5-year snapshots before 2000; annual after 2000**	**Zhang et al. (2024)**
ESA WorldCover	10 m	2020, 2021	Single-year maps	Zanaga et al. (2021, 2022)
ESA CCI Land Cover / C3S LC	300 m	1992–2022	Annual	UCL-Geomatics / ESA CCI (2022)
MODIS MCD12Q1	500 m	2001–2024	Annual	Friedl and Sulla-Menashe (2022)
GlobeLand30	30 m	2000, 2010, 2020	Decadal epochs	Chen et al. (2015)
Copernicus Global Land Cover	100 m	2015–2019	Annual	Buchhorn et al. (2020)
Dynamic World	10 m	2015–present	Near-real-time	Brown et al. (2022)

Manuscript revision: Lines 248-254, Section 2.2.

New text:

The resulting layers should therefore be interpreted as GLC_FCS30D-based land-cover transition products rather than as direct spectral–temporal breakpoint products. GLC_FCS30D was selected because, among currently available land-cover products, it uniquely combines global coverage, 30 m spatial resolution, annual temporal resolution after 2000, and an extended historical record back to 1985, which constitutes the combination of properties required for long-term, fine-resolution, global mining-dynamic analysis.

Comment 2: Inherited classification uncertainty of LULC maps

Reviewer's Comment: *" Disturbance estimates inherit uncertainties from GLC_FCS30D,* *including class confusion, regional classification bias, and thematic inconsistency. Rule-based thresholds introduce additional assumptions that may further compound uncertainty."*

Response: We agree with the referee. The DEV and REC layers in our dataset are derived from GLC_FCS30D land-cover transitions inside known mining boundaries, so any classification artefact in the source product propagates into our outputs. Sources of inherited uncertainty include confusion between bare-soil cropland and mine-related bare surfaces, regional bias in arid or sparsely vegetated environments, and the temporal-consistency procedures applied during land-cover production. The rule-based transition criteria translate categorical class transitions into "development" and "reclamation" events through fixed class groupings, which adds a further interpretive layer. To address the referee's concern, we have rewritten Section 4.3 so that this inheritance chain is explicit, and we have added a quantitative cross-product sensitivity assessment that bounds how strongly the inferred mining transitions depend on the choice of source land-cover product. **Within the 27,948 Chinese mining polygons over 2001–2022, CLCD recovered 80.9 % of the GLC_FCS30D-based development area and 25.9 % of the reclamation area, with co-detection rates of 67.6 % and 37.6 % and median transition-year offsets of 2.97 and 6.71 years, respectively. This bounds the component of dataset uncertainty attributable to the source LULC product: development estimates are comparatively transferable across products, while reclamation timing is markedly more sensitive to product choice.**

For the cross-product reference we used the China Land Cover Dataset (Yang and Huang, 2021). CLCD shares GLC_FCS30D's 30 m native resolution, provides annual maps over 1985–2025, and is produced independently of GLC_FCS30D using a different 9-class scheme and different temporal-consistency rules. These three properties are jointly required for a meaningful cross-product comparison of mining-related transitions. We restricted the comparison window to 2001–2022 because GLC_FCS30D is delivered as five-year snapshots before 2000 (1985, 1990, 1995) and as annual maps thereafter; pairing CLCD's annual maps with the pre-2000 five-year era of GLC_FCS30D would primarily reflect this temporal-resolution mismatch rather than classifier-driven differences. Among other 30 m global or near-global land-cover products, ESA WorldCover provides only single-year maps (2020, 2021), and country-specific products such as MapBiomas (Brazil and others) and the USGS National Land Cover Database (contiguous United States) do not cover China. CLCD therefore provides the closest available match for our purposes within its native China scope. China is also a demanding test region: it concentrates 27,948 of the 74,726 mining polygons in our dataset, spans diverse mining types and ecoclimatic zones, and includes regions where GLC_FCS30D's classifier confusion is most likely to surface (north-western arid zones, transitional grasslands, peri-urban industrial areas).

The validation applies the same conceptual transition rule used for the GLC_FCS30D-based DEV/REC layers, mapped to CLCD's own class system. A pixel was assigned a development year y if it was classified as a mine-related class at year y and as a vegetation/cropland class at year y−1; a reclamation year y if the converse held. The earliest year satisfying the condition within the comparison window was retained. This is the relative-year rule used in the GLC_FCS30D workflow. Class equivalence was set as follows. In CLCD, the mine-related class group comprised classes 5 (Water), 7 (Barren) and 8 (Impervious), matching the impervious, bare and water grouping used in the GLC_FCS30D-based mine-related class. The vegetation/cropland class group comprised CLCD classes 1 (Cropland), 2 (Forest), 3 (Shrub), 4 (Grass) and 9 (Wetland), matching the cropland and vegetation classes used in our workflow. Transition detection itself was performed at the 30 m pixel level for both products, using the rule described above. The resulting per-pixel transition years were then aggregated to the 27,948 Chinese mining polygons of our dataset over 2001–2022 to enable cross-product comparison. For each polygon and each transition type (DEV, REC), we recorded separately for each product the total transition area (cumulative valid-pixel area) and the area-weighted mean transition year. From these polygon-level summaries we derived three classes of agreement metric, reported in Table R2: polygon-level co-detection, cumulative transition area, and polygon-mean transition-year offset.

Table R2. Object-level cross-product comparison between CLCD and GLC_FCS30D in Chinese mining polygons, 2001–2022. Temporal-agreement metrics are computed between two independently produced 30 m LULC products at the polygon scale; they bound the part of transition-year uncertainty attributable to the choice of source land-cover product, and should not be interpreted as accuracy estimates against ground truth.

Metric	DEV	REC
Polygon-level co-detection (n = 27,948)		
Co-detected by both products	18,906 (67.6 %)	10,507 (37.6 %)
Detected by GLC_FCS30D-based workflow only	5,141 (18.4 %)	13,273 (47.5 %)
Detected by CLCD only	532 (1.9 %)	386 (1.4 %)
Detected by neither	3,369 (12.1 %)	3,782 (13.5 %)
Cumulative transition area (2001–2022)		

GLC_FCS30D-based workflow (km^2)	4,210.97	3,058.53
CLCD (km^2)	3,407.89	790.94
CLCD / GLC_FCS30D area ratio (%)	80.9	25.9
Polygon-mean transition-year offset (co-detected polygons only)		
Mean (yr)	3.81	7.18
Median (yr)	2.97	6.71
Polygons agreeing within ±2 yr (%)	36.4	13.5
Polygons agreeing within ±5 yr (%)	72.0	37.0

From the validation results, we draw the following conclusions.

First, the CLCD comparison provides a same-resolution test of how sensitive the workflow is to the choice of source LULC product. Within the 27,948 Chinese mining polygons over 2001–2022, the GLC_FCS30D-based workflow detected 4,210.97 km² of mining development and 3,058.53 km² of reclamation, whereas CLCD detected 3,407.89 km² and 790.94 km² under the same conceptual transition rule. These correspond to 80.9 % and 25.9 % of the GLC_FCS30D-based estimates, respectively. Thus, development is relatively more consistent across the two independent 30 m LULC products, while reclamation is much more sensitive to the choice of source product. The polygon-level results show the same pattern: 18,906 polygons (67.6 %) were co-detected for development and 10,507 (37.6 %) for reclamation, while GLC_FCS30D-only detections were much more frequent for reclamation (13,273 polygons; 47.5 %) than for development (5,141 polygons; 18.4 %). This difference provides a quantitative bound on the component of uncertainty attributable to the source LULC product, especially for reclamation.

This contrast is consistent with both the nature of the mining transitions and methodological differences between the two LULC products. Mining development is usually an abrupt and spatially coherent conversion from vegetation or cropland to bare or artificial surfaces, making it more readily detected by independent annual LULC products. Reclamation, by contrast, is often a gradual multi-year revegetation process that passes through sparse-vegetation or mixed land-cover states, which may not produce a clear year-to-year class change. From a methodological perspective, GLC_FCS30D uses continuous change detection on multi-decadal Landsat reflectance time series to identify breakpoints in pixel-level spectral trajectories (Zhu and Woodcock, 2014; Zhang et al., 2024). CLCD is generated from annual Random Forest classifications followed by temporal-consistency processing (Yang and Huang, 2021), which improves map stability and reduces single-year noise but may also smooth or delay gradual transitions. In addition, GLC_FCS30D provides more detailed bare, impervious, and water-related classes relevant to mining landscapes, whereas CLCD uses broader Barren and Impervious categories. These differences help explain why GLC_FCS30D was selected as the source LULC product in this study and how the detected mining and reclamation changes are affected by the choice of LULC dataset.

Second, the disagreement between the two products is strongly directional. CLCD-only polygons accounted for only 532 development cases (1.9 %) and 386 reclamation cases (1.4 %), compared with 5,141 development cases (18.4 %) and 13,273 reclamation cases (47.5 %) detected only by the GLC_FCS30D-based workflow. Therefore, CLCD rarely detected transitions in polygons where the GLC_FCS30D-based workflow detected none. Most differences instead arose from transitions detected by the GLC_FCS30D-based workflow but not by CLCD. This directional pattern does not by itself prove that all additional GLC_FCS30D-based detections are correct, but it indicates that the discrepancy is mainly associated with higher sensitivity of the GLC_FCS30D-based workflow rather than widespread bidirectional disagreement between products.

Third, temporal agreement was also stronger for development than for reclamation. Among co-detected development polygons, the median polygon-mean transition-year offset was 2.97 years, and 72.0 % of polygons agreed within ±5 years. Reclamation showed larger temporal offsets, with a median difference of 6.71 years and only 37.0 % of co-detected polygons agreeing within ±5 years. This larger offset is consistent with reclamation being a gradual greening process rather than a discrete disturbance event. Therefore, reclamation timing in the dataset should be interpreted more cautiously than development timing, and reclamation estimates are best viewed as remote-sensing indicators of land-cover recovery rather than field-confirmed dates of completed ecological restoration. Importantly, these polygon-mean transition-year offsets are not ground-truth accuracy estimates. They quantify how the inferred timing of mining transitions shifts when the source LULC product is changed from GLC_FCS30D to CLCD. This product-level comparison complements the pixel-level temporal validation in Section 2.4: the sample-based validation evaluates transition-year accuracy against trajectory-based reference evidence, whereas the CLCD comparison estimates uncertainty attributable to the choice of source LULC product. We also updated the overall description of the validation strategy in Section 2.4 and revised the workflow in Figure 1 accordingly (lines 166, section 2). These changes are reflected in the revised manuscript.

Manuscript revision: Lines 337-347, Section 2.4.

Original text:

To comprehensively evaluate the performance of the proposed method, we designed a dual-track validation framework addressing both spatial accuracy and temporal accuracy. The spatial validation focuses on assessing the reliability of mining area delineation by comparing our refined dataset with two existing global mining datasets through stratified cross-validation across four spatially defined zones. The temporal validation targets the accuracy of mining-reclamation transition year detection through multi-index spectral trajectory analysis over a 25-year period (1990–2022). Both validation components employed stratified random sampling and integrated high-resolution Google Earth imagery with Landsat/Sentinel-derived spectral indices for reference label generation.

Revised text:

The validation and sensitivity-assessment framework includes three ways to evaluate the performance and uncertainty of the proposed method: spatial validation, temporal validation, and cross-product sensitivity assessment. The spatial validation assessed the reliability of mining-area delineation by comparing our refined dataset with two existing global mining datasets through stratified cross-validation across four spatially defined zones. The temporal validation evaluated transition-year accuracy at sampled 30 m pixels using high-resolution Google Earth imagery, Landsat-based spectral trajectories with reference to the LandTrendr segmentation. The cross-product sensitivity assessment compared the GLC_FCS30D-based workflow with the same conceptual transition rules applied to CLCD over Chinese mining polygons, thereby quantifying uncertainty attributable to the choice of source LULC product.

Manuscript revision: Lines 165, Section 2.

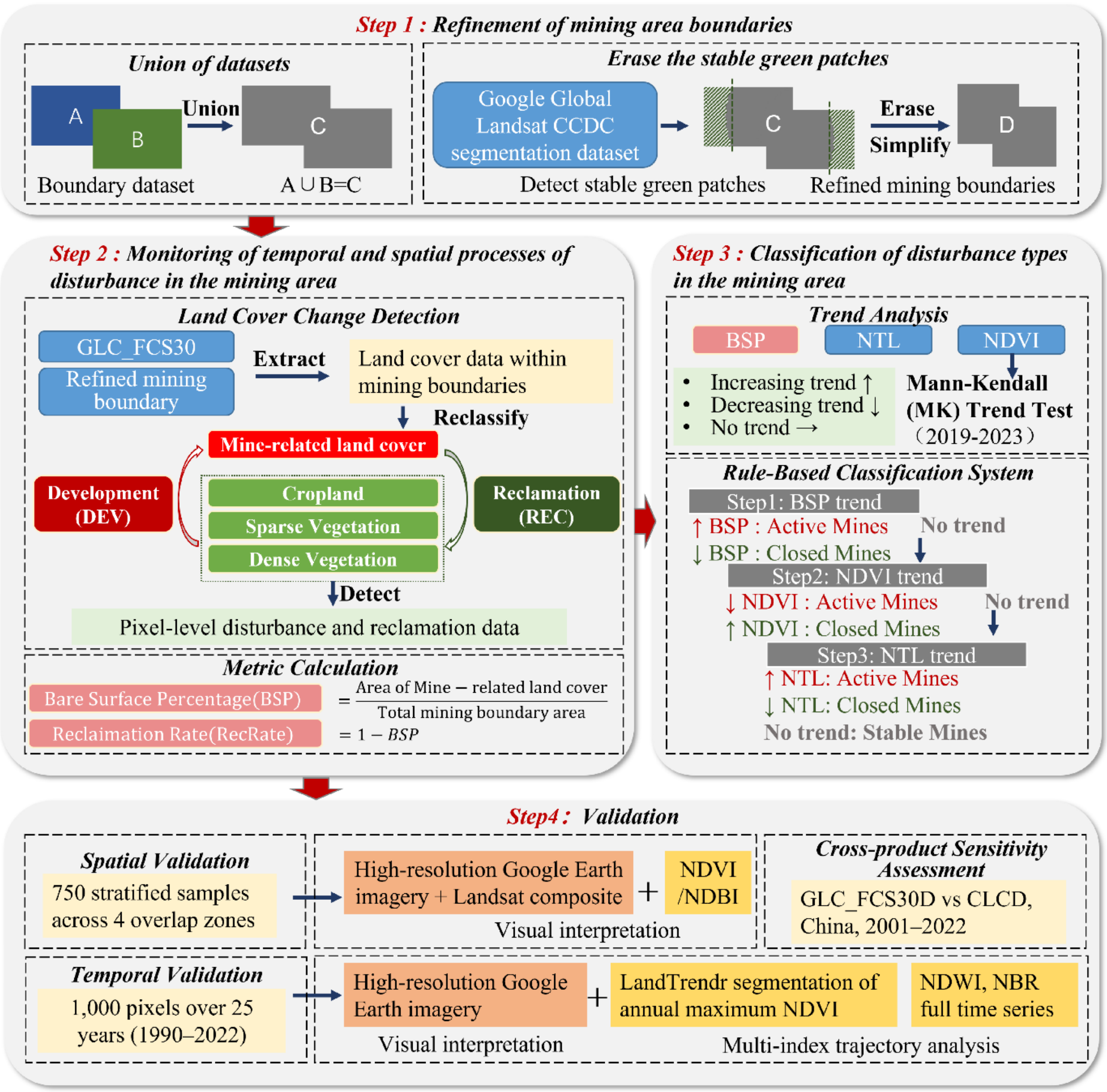

Manuscript revision: Lines 423-441, Section 2.4.

New text:

In addition, to assess how strongly the inferred mining transitions depend on the choice of source land-cover product, we performed an object-based cross-product sensitivity assessment using the China Land Cover Dataset (Yang and Huang, 2021). CLCD provides 30 m annual maps over 1985–2025 for China, classified independently of GLC_FCS30D using a 9-class scheme and distinct temporal-consistency rules. The comparison was restricted to the 27,948 Chinese mining polygons of our dataset over 2001–2022, the temporal window in which both products provide annual maps; the pre-2000 period was excluded because GLC_FCS30D is delivered as five-year snapshots there (1985, 1990, 1995), and a comparison with CLCD's annual maps in that period would primarily reflect this temporal-resolution mismatch rather than classifier-driven differences. We applied the same conceptual transition rule used for the

GLC_FCS30D-based DEV/REC layers, with class equivalence mapped to CLCD's class system. In CLCD, the mine-related class group comprised classes 5 (Water), 7 (Barren) and 8 (Impervious), and the vegetation/cropland class group comprised classes 1 (Cropland), 2 (Forest), 3 (Shrub), 4 (Grass) and 9 (Wetland). For each mining polygon we recorded, separately for development and reclamation, the total transition area in each product, the area-weighted mean transition year in each product, the polygon-level co-detection status, the area ratio CLCD/GLC_FCS30D, and the absolute polygon-mean transition-year offset between products in co-detected polygons.

Manuscript revision: Lines 876-901, Section 4.3.

New text:

The CLCD comparison provides a same-resolution assessment of the dependence of our workflow on the source LULC product and helps clarify the added information gained from using GLC_FCS30D. Over Chinese mining polygons during 2001–2022, the GLC_FCS30D-based workflow detected 4,211 km² of development and 3,058.5 km² of reclamation, whereas CLCD detected 3,407.9 km² and 790.9 km² under the same conceptual transition rule, corresponding to 80.9 % and 25.9 % of the GLC_FCS30D-based estimates, respectively. At the polygon level, 67.6 % of polygons were co-detected for development, compared with 37.6 % for reclamation; CLCD-only detections were rare, accounting for only 1.9 % of development polygons and 1.4 % of reclamation polygons, while GLC_FCS30D-only detections accounted for 18.4 % and 47.5 %, respectively. For co-detected polygons, the median offsets in the area-weighted mean transition year were 2.97 years for development and 6.71 years for reclamation. This directional pattern indicates that most transitions detected by CLCD were also captured by the GLC_FCS30D-based workflow, whereas the latter identified many additional within-polygon changes, particularly for reclamation. These differences likely reflect both the nature of mining transitions and the design of the source LULC products: development is usually an abrupt conversion to bare or artificial surfaces, while reclamation is often gradual and fragmented; meanwhile, GLC_FCS30D uses continuous change detection on multi-decadal Landsat reflectance time series and provides more detailed bare, impervious, and water-related classes, whereas CLCD is based on annual Random Forest classifications with temporal-consistency processing and broader land-cover categories (Yang and Huang, 2021; Zhu and Woodcock, 2014; Zhang et al., 2024). These results support the use of GLC_FCS30D as the source LULC product in this study and quantify how the detected mining and reclamation changes are affected by the choice of LULC dataset.

Comment 3: Temporal resolution constraints

Reviewer's Comment: *"Mining dynamics are often highly non-linear and abrupt, whereas the dataset relies on annual classifications after 2000 and five-year intervals before 2000. This temporal aggregation may smooth short-term fluctuations, delay disturbance detection, and affect annual area estimates, particularly in the early period."*

Response: We agree. We have revised both the Methods and the Discussion to make this temporal limitation explicit. In the early period of Landsat program, the observation is extremely uneven distributed due to commercial interest. Pre-2000 transition years are interpolated from five-year GLC_FCS30D maps and should be interpreted as interval-based estimates rather than directly observed annual changes. We also clarify that even after 2000, when annual maps are available, the assigned transition year may lag the physical disturbance because land-cover products apply classification and temporal-consistency procedures that favor stable class labels over single-year flips. The annual DEV/REC areas should therefore be read as land-cover-transition estimates rather than as exact operational mining or reclamation records.

Manuscript revision: Lines 245-248, Section 2.2.

Original text:

GLC_FCS30D dataset provides maps with a five-year frequency from 1985 to 2000 and annually thereafter. Thus, we performed time interpolation on the data from before 2000.

Revised text:

GLC_FCS30D provides maps at five-year intervals before 2000 and annually thereafter. Pre-2000 transition timing was therefore interpolated, and annual area estimates before 2000 should be interpreted as interval-averaged estimates rather than directly observed annual changes.

Comment 4: Implications: robustness tied to GLC_FCS30D quality and stability

Reviewer's Comment: *"Given these dependencies, the robustness of the dataset is closely tied to the quality and stability of GLC_FCS30D. A clearer discussion, and ideally a quantitative assessment, of uncertainty propagation and temporal limitations would strengthen confidence in the dataset's validity."*

Response: Thank you for this important suggestion. We fully agree, and the revisions address this concern through both quantitative and discursive changes. The cross-product sensitivity assessment described under Comment 2 provides a numerical estimate of how strongly the inferred mining transitions depend on the choice of source land-cover product. Within the 27,948 Chinese mining polygons over 2001–2022, CLCD recovered 80.9 % of the GLC_FCS30D-based development area and 25.9 % of the reclamation area, with median polygon-mean transition-year offsets of 2.97 years for development and 6.71 years for reclamation. The disagreement between the two products was strongly directional: CLCD-only detections accounted for only 1.9 % of polygons for development and 1.4 % for reclamation, against 18.4 % and 47.5 % for GLC_FCS30D-only detections. Together, these metrics establish a quantitative bound on the component of dataset uncertainty attributable to the choice of source LULC product. The full numerical results, methodology, and discussion are presented in our response to Comment 2 and in Section 4.3 of the revised manuscript.

Response to Report #2 - Anonymous referee #3

Major Comment 1: Potential limitation in detecting previously unmapped mining areas

Reviewer's Comment: *"The proposed dataset is constructed through the integration and refinement of two existing global mining datasets. While the workflow and results clearly improves boundary delineation and achieves finer spatial representation, it appears fundamentally constrained by the completeness of the input datasets. Specifically, there are cases where certain mining areas are not included in either of the original datasets. As shown in Figure 2, a portion of the mining area (e.g., the upper-left region of the example site) is not identified in both source datasets, and consequently remains absent in the final refined dataset. This suggests that the current approach mainly enhances the geometric precision of already identified mining regions, but lacks the ability to detect previously omitted areas. Therefore, the dataset may primarily improve boundary accuracy rather than spatial completeness. This limitation should be explicitly acknowledged and discussed, particularly in the context of global-scale applications."*

Response: We thank the referee for this careful and accurate observation, and we agree. The integration workflow is designed to refine, harmonize, and remove overestimated portions of known mining footprints in the two source inventories (Maus et al., 2022; Tang and Werner, 2023); it is not designed to discover mining sites absent from both sources. The Figure 2 example illustrates this honestly: where neither source captured a mining patch, our workflow cannot recover it. We have revised both the Methods and the Discussion to state this scope limitation explicitly and to reframe the final boundary product as a refined boundary "conditional on the completeness of the input mining inventories." We have also indicated, in the Discussion, the three regimes most likely to be affected: (i) newly developed mines after the circa-2020 source delineation date; (ii) small or informal/artisanal mining sites below the spatial-detection threshold of either source; and (iii) regions where both source inventories share systematic omissions (e.g., certain artisanal-mining belts). Future work integrating time-series mining-site discovery (for example the tropical mining product of Sepin et al., 2025, or dedicated change-based detection workflows) would be needed to address this limitation, and we have added a forward-looking note to that effect.

Manuscript revision: Lines 177-182, Section 2.1.

New text: This integration step relies on the spatial coverage of the two source mining inventories. The workflow is therefore designed to refine, harmonize, and remove overestimated portions of known mining areas, rather than to perform global discovery of mining sites absent from both input datasets. Mining areas that are missing from both sources cannot be recovered by the integration step and remain absent from the refined boundary product.

Location: Lines 903–919, Section 4.3.

Original text:

A further methodological consideration is the use of static mining boundaries. Our analysis was conducted within the maximum union of two pre-existing global mining datasets, which provides comprehensive spatial coverage but cannot capture mining activities that expanded beyond these boundaries during the study period. It should be noted that these boundaries are static and derived from satellite imagery circa 2020. Newly developed mining areas not represented in the source datasets (Maus et al., 2022; Tang and Werner, 2023) are necessarily excluded from our analysis. Future work integrating time-series boundary delineation methods could address this limitation and provide a more complete picture of mining's evolving spatial footprint.

Revised text:

A further methodological consideration is the use of static mining boundaries together with pre-existing mining inventories. Our analysis was conducted within the union of two published global mining datasets (Maus et al., 2022; Tang and Werner, 2023). This design improves boundary precision and reduces overestimated non-mining areas within known mining footprints, but it cannot discover mining sites absent from both source datasets. The "maximum potential mining disturbance boundary" used in this study should therefore be understood as a refined boundary conditional on the completeness of the input inventories. Newly developed mines after the circa-2020 source delineation date, small or informal/artisanal mining sites below the spatial-detection threshold of either source, and regions where both inventories share systematic omissions (e.g., certain artisanal-mining belts) may be under-represented or missing from the refined dataset. Consequently, our dataset primarily enhances the geometric precision of already identified mining regions and improves spatial consistency rather than spatial completeness; users applying the dataset for global mining-area accounting should account for this scope. Future work integrating time-series mining-site discovery methods could address this limitation and provide a more complete picture of mining's evolving spatial footprint.

Major Comment 2: Concerns regarding the temporal validation strategy

Reviewer's Comment: *Although the authors have supplemented quantitative validation in response to previous comments, there are still concerns regarding the robustness of the temporal validation design. As stated in Line 364, "For each year within the sampling period, 40 mining-related pixels were randomly selected using a stratified sampling strategy." First, for a global-scale dataset, selecting 40 samples per year is relatively limited and may reduce the statistical reliability of the validation results. More importantly, the samples are independently drawn for each year, meaning that most locations are not consistently tracked over time. As a result, the validation primarily reflects per-year classification accuracy rather than the accuracy of temporal trajectories or transition timing. Given that this study emphasizes spatiotemporal dynamics as a key contribution, such a validation strategy is insufficient to demonstrate the reliability of temporal changes. It also does not adequately address the potential limitation discussed above regarding the omission of mining areas.*

Response:

We thank the referee for this careful comment. We agree that the original wording in Section 2.4 did not sufficiently explain the temporal validation design, especially the distinction between per-year classification accuracy and transition-year accuracy. We have revised Section 2.4 to describe the sampling design and interpretation procedure more clearly.

The 1,000 reference samples were drawn from mining-related 30 m pixels for which our dataset reports a development or reclamation transition. To maintain temporal balance across the study period, 40 pixels were randomly selected for each of 25 nominal transition years or time steps (1990, 1995, and 2000–2022). Each selected pixel was not interpreted only for the sampled year, but for the full multi-decadal temporal trajectory. Because the vegetation loss induced by mining can not occurs twice (or more) during the study timeframe, the year which has the greatest probability of mining development in the whole temporal trajectory was assigned an independent reference transition year. This interpretation was based on the available high-resolution Google Earth imagery time series, Landsat-based spectral trajectories, and LandTrendr segmentation of annual maximum NDVI. The metric reported in Figure A7 is therefore the offset between the transition year predicted by our dataset and the trajectory-derived reference transition year, evaluated under explicit temporal tolerance windows.

We have clarified this point because per-year classification accuracy and transition-year accuracy are different quantities. Per-year classification accuracy asks whether the land-cover class in a particular year matches a reference label for that same year. Transition-year accuracy asks whether the timing of a detected state change corresponds to the timing inferred from the full temporal trajectory. Our validation follows the latter logic. The fact that samples were independently drawn for each nominal transition year affects which pixels are included in the validation set, but it does not mean that each pixel was assessed only in one single year. Rather, the stratification was used to ensure that early and recent transition periods were both represented in the validation set.

We also clarify that this validation evaluates the combined temporal performance of our transition-detection workflow, including both the source GLC_FCS30D land-cover time series and the rule-based DEV/REC transition criteria. The general land-cover classification accuracy of GLC_FCS30D has been reported in the source product paper, with an overall accuracy of 80.88 % for the 10-class system and 73.04 % for the LCCS level-1 system (Zhang et al., 2024). Our validation is complementary to that product-level assessment: it specifically examines whether the mining-related transition years inferred by our workflow are consistent with independent trajectory-based reference evidence at sampled pixels. In addition, as described in our response to Referee #1, we added a CLCD-based cross-product sensitivity assessment to quantify the uncertainty attributable to the choice of source LULC product.

We acknowledge that 1,000 samples remains limited for a global dataset. Therefore, we complemented the sample-based temporal validation with a cross-product sensitivity assessment using CLCD, which covers more than 27,000 mining polygons in China. We did not expand the sample size in this revision because trajectory-based interpretation is substantially more time-consuming than single-year visual labelling: each sample requires examination of the full multi-decadal record using multi-source imagery and spectral trajectories. Within the revision period, we prioritized balanced temporal coverage across the 25 nominal transition years rather than enlarging the total sample size at the expense of temporal balance. We have now stated this limitation explicitly in Section 4.3 and identified expansion of the trajectory-based reference sample set as a future improvement.

Finally, we agree that the temporal validation does not address the spatial-omission issue raised in Major Comment 1. Temporal validation evaluates whether the predicted transition year is consistent with the trajectory-derived reference year at sampled mining-related pixels; it cannot test whether mining areas omitted from both source inventories can be recovered. We have explicitly acknowledged this limitation in our response to Major Comment 1 and revised the manuscript accordingly (Section 2.1 and Section 4.3).

Manuscript revision: Lines 381-402, Section 2.4.

Original text：

We conducted stratified random sampling over 25 years (1990, 1995, and 2000-2022) to assess the temporal accuracy of the proposed method in detecting mining-reclamation transition years. For each year within the sampling period, 40 mining-related pixels were randomly selected using a stratified sampling strategy, resulting in a total of 1,000 validation samples. Figure. A2 shows the spatial distribution of all validation samples. Reference labels were generated through visual interpretation of high-resolution Google Earth imagery. To enhance the consistency and accuracy of interpretation, LandTrendr-derived segmentation of the annual maximum NDVI time series was integrated, along with complementary spectral profiles from Normalized Difference Water Index (NDWI) and Normalized Burn Ratio (NBR) indices. All three indices (NDVI, NDWI, and NBR) were derived from Sentinel-2 MSI surface reflectance data.

Revised text：

To assess the accuracy of the detected transition years, we constructed a reference set of 1,000 samples drawn from mining-related pixels at which the dataset reports a development or reclamation transition. To maintain temporal balance across the study window, 40 pixels were randomly selected for each of 25 nominal transition years or time steps (1990, 1995, and 2000–2022), giving a total of 1,000 validation samples whose spatial distribution is shown in Figure A2. Reference transition years were assigned through visual interpretation of the available high-resolution Google Earth imagery time series, supported by Landsat-based spectral trajectories. Specifically, we used Landsat Collection 2 Level-2 surface reflectance data from Landsat 4, 5, 7, 8, and 9 for the period 1985–2024. Surface reflectance values were scaled using the Collection 2 scale factors, and clouds, cloud shadows, and saturated pixels were masked using the QA_PIXEL and QA_RADSAT bands. For each valid Landsat observation, we calculated NDVI together with complementary Normalized Difference Water Index (NDWI) and Normalized Burn Ratio (NBR) to assist the interpretation of disturbance and recovery signals. Annual maximum NDVI composites were further generated and segmented using the LandTrendr algorithm to identify major breakpoints in the vegetation trajectory. The final reference transition year for each validation sample was determined by jointly considering the high-resolution imagery record, the LandTrendr segmentation result, and the multi-year Landsat spectral-index profiles. The accuracy metric reported in Figure A7 is the offset between the dataset's predicted transition year and the trajectory-derived reference transition year, evaluated under explicit temporal tolerance windows.

Manuscript revision: Lines 1008-1013, Section 4.3.

New text:

The temporal validation sample set provides an overview of global accuracy across biomes. Although the 1,000 samples were temporally balanced across 25 nominal transition years or time steps, future work should expand the trajectory-based reference sample set and further stratify it by region, biome, mine type, and transition type to better characterize temporal uncertainty across different mining contexts.

Major Comment 3: Spatial scale inconsistency between mining boundaries and MODIS data

Reviewer's Comment: *"There is a notable spatial scale inconsistency between the high-resolution mining boundaries and the MODIS-based NDVI data used in the analysis. Given the relatively coarse spatial resolution of MODIS, it is likely that individual pixels contain a mixture of mining and non-mining land cover, especially for smaller mining polygons. This introduces a mixed-pixel effect, which may bias the estimation of vegetation dynamics and, consequently, affect the interpretation of mining disturbance and reclamation processes.*

Additionally, Landsat imagery is already used in the study (e.g., Figure 4). It is therefore unclear why Landsat-based NDVI (with a higher spatial resolution) was not adopted for the main analysis during periods when Landsat data are available. Using higher-resolution data could significantly improve spatial consistency and reduce uncertainty."

Response: We thank the referee for this important comment. We agree that the spatial mismatch between high-resolution mining boundaries and MODIS NDVI can introduce mixed-pixel effects, especially for small mining polygons. We also recognize that the original manuscript did not clearly distinguish the two different uses of NDVI in the study: MODIS NDVI was used for recent polygon-level status classification in Section 2.3, whereas Landsat-based spectral trajectories were used for the 30 m pixel-level temporal validation in Section 2.4 and Figure 4. We have revised the manuscript to make this distinction explicit.

First, MODIS NDVI is not used to construct the 30 m development (DEV) or reclamation (REC) area and year layers. These primary spatiotemporal products are derived from GLC_FCS30D land-cover transitions within mining boundaries, as described in Section 2.2. MODIS NDVI does not enter the DEV/REC mapping workflow at any stage, and therefore does not affect the 30 m mining disturbance and reclamation time-series layers released in this study.

Second, MODIS NDVI is used only as one of three indicators for recent polygon-level status classification in Section 2.3. For this analysis, we extracted three annual polygon-level indicators: bare surface proportion (BSP), NDVI, and nighttime lights (NTL). BSP was derived at 30 m from GLC_FCS30D; NDVI was derived from the MODIS Collection 6.1 MOD13Q1 and MYD13Q1 250 m vegetation-index products by merging Terra and Aqua observations and calculating annual maximum NDVI for 2019–2023; and NTL was derived from VIIRS nighttime-light observations. For each indicator, annual mean values were summarized within each mining polygon and used as input to the Mann–Kendall trend test. Thus, the trend test is performed at the mining-polygon scale rather than by interpreting individual MODIS pixels as pure mining pixels. This aggregation reduces, but does not eliminate, the influence of edge mixed pixels. The status classification also does not rely on MODIS NDVI alone, because it combines MODIS NDVI with 30 m BSP and NTL as an independent human-activity indicator.

We used MODIS NDVI for this polygon-level status indicator because the analysis requires globally consistent annual vegetation summaries for tens of thousands of mining polygons distributed across diverse biomes. The Terra/Aqua MODIS vegetation-index products provide high temporal sampling and stable global coverage, which helps reduce cloud-related and seasonal sampling gaps when producing annual-maximum NDVI composites. Landsat was instead used in the validation step, where 1,000 sampled 30 m pixels were interpreted individually using high-resolution Google Earth imagery and detailed Landsat spectral trajectories. Constructing an equivalent global Landsat-based polygon-level NDVI product for the status classification is possible in principle, but would require additional processing to address Landsat 7 SLC-off gaps, cloud and shadow contamination in persistently cloudy regions, cross-sensor consistency among Landsat 7/8/9, gap handling, and regionally varying seasonality. We therefore used Landsat where 30 m pixel-level validation evidence was required, and MODIS NDVI where a robust global polygon-level status indicator was needed. We have clarified this rationale in the revised manuscript and identified harmonized Landsat–Sentinel vegetation-index time series as an important direction for future improvement.

We also found that the original manuscript incorrectly stated that the spectral indices used in the validation were derived from Sentinel-2 MSI surface reflectance data. This was an inadvertent wording error. The validation spectral profiles were in fact derived from Landsat Collection 2 Level-2 surface reflectance data from Landsat 4, 5, 7, 8, and 9 over 1985–2024. We have corrected this statement in the revised manuscript and listed it explicitly in the Additional Author Revisions.

Finally, we agree that MODIS NDVI mixed-pixel effects remain a limitation for very small or narrow mining polygons. Although polygon-level aggregation and the combined use of BSP, NDVI, and NTL reduce the dependence on any single MODIS pixel, they cannot fully remove spatial-scale mismatch. We have added this caveat to Section 4.3 and noted that future versions could improve recent status classification by using harmonized Landsat–Sentinel vegetation-index time series or other higher-resolution global vegetation products.

Manuscript revision: Lines 291-292, Section 2.3.

New text:

These indicators were then aggregated within each mining polygon to construct polygon-level annual time series for the Mann-Kendall trend analysis.

Manuscript revision: Lines 951-971, Section 4.3.

Original text:

NDVI saturation effects in medium-to-high biomass environments (typically where NDVI > 0.8) may reduce sensitivity to vegetation recovery trends, particularly in densely vegetated reclamation sites within tropical biomes. Although the GLC_FCS30D land-cover classification employed in this study integrates multiple spectral and temporal features that partially alleviate reliance on a single vegetation index, the MODIS-derived NDVI time series used for recovery trend analysis may still underestimate vegetation regrowth under closed-canopy conditions.

Alternative indicators such as NIRv (near-infrared reflectance of vegetation), which maintains sensitivity at high leaf area index (Badgley et al., 2017, 2019), or nonlinear variants such as kNDVI, could provide more accurate characterization of recovery trajectories. Future regional-scale assessments, especially in tropical forest environments, should consider incorporating NIRv-based trend analysis to better capture advanced stages of ecological reclamation.

Revised text:

The MODIS-derived NDVI time series used for recent status classification has two main limitations. First, although NDVI was aggregated at the mining-polygon scale rather than interpreted as pure 250 m pixels, mixed-pixel effects may still affect small or narrow mining polygons where MODIS pixels include both mining and surrounding non-mining land cover. This spatial-scale mismatch may influence the estimated vegetation trend used for status classification, but it does not affect the 30 m DEV/REC area and year layers, which are derived from GLC_FCS30D land-cover transitions. Second, NDVI saturation effects in medium-to-high biomass environments (typically where NDVI > 0.8) may reduce sensitivity to vegetation recovery trends, particularly in densely vegetated reclamation sites within tropical biomes. Although the GLC_FCS30D land-cover classification employed in this study integrates multiple spectral and temporal features that partially alleviate reliance on a single vegetation index, the MODIS-derived NDVI time series used for recovery trend analysis may still underestimate vegetation regrowth under closed-canopy conditions. Alternative indicators such as NIRv (near-infrared reflectance of vegetation), which maintains sensitivity at high leaf area index (Badgley et al., 2017, 2019), or nonlinear variants such as kNDVI, could provide more accurate characterization of recovery trajectories. Future regional-scale assessments, especially in tropical forest environments or small and fragmented mining areas, should consider incorporating NIRv-based or harmonized Landsat-Sentinel vegetation-index time series to better capture advanced stages of ecological reclamation and reduce mixed-pixel uncertainty.

Minor Comments

1. **Reviewer's Comment:** *"The readability of Figure 4 is limited, particularly the text and axis labels in the line plots, which are difficult to interpret."*

Response: Thank you for pointing this out. We have revised Figure 4 to improve the readability of the spectral-trajectory panels. Specifically, we increased the font sizes of the axis labels, tick labels, and legends in the line plots so that they remain legible at the published figure size. We also added a clearer annotation for the red vertical line indicating the LCTS mining year. These changes improve the interpretability of the figure without altering the underlying data or analysis.

Manuscript revision: Lines 411, Section 2.4.

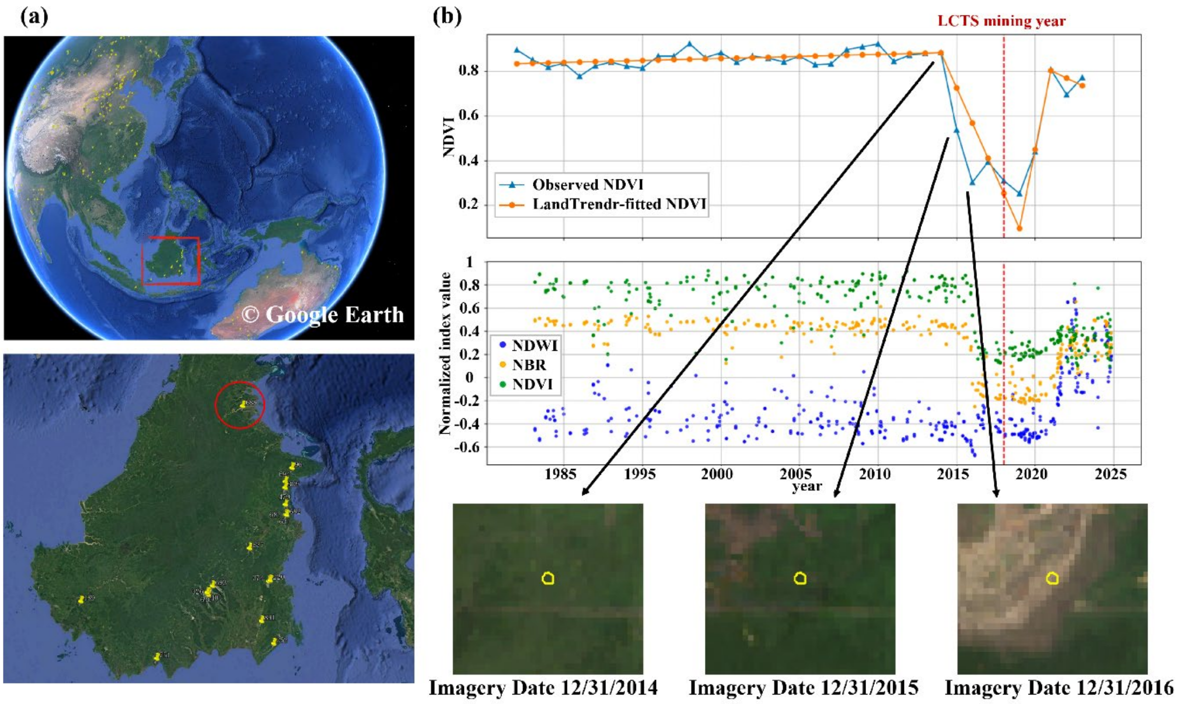

2. **Reviewer's Comment:** *"There appears to be a potential inconsistency in the temporal coverage. The dataset is described as spanning 1985–2022, whereas Line 263 refers to trends up to 2023. Please clarify whether data from 2023 are included or if this is a wording issue."*

Response:

We thank the referee for catching this ambiguity. The two time periods refer to different components of the analysis, but this distinction was not sufficiently clear in the original manuscript.

The released DEV/REC area and year layers cover 1985–2022. This temporal range is determined by the availability of GLC_FCS30D, which is the source land-cover product used to derive the 30 m development and reclamation transition layers in Section 2.2. The DEV/REC dataset was not extended to 2023 because a corresponding 2023 GLC_FCS30D annual layer was not available for this workflow.

The reference to 2023 concerns only the recent polygon-level status classification in Section 2.3. This analysis is not used to generate the DEV/REC area or year layers; rather, it uses auxiliary indicators to characterize the current operational status of mining polygons. We used a short recent window for this analysis because the aim was to distinguish current status, such as active expansion, reclamation, or stability, rather than to summarize the full historical trajectory. A longer window would risk mixing earlier mining phases with the present operational state. For this reason, we used the most recent observations included in our status-classification analysis for each auxiliary indicator: BSP from GLC_FCS30D for 2019–2022, and MODIS NDVI and VIIRS NTL for 2019–2023. Including the 2023 NDVI and NTL observations improves the recency of the vegetation and human-activity signals used for status classification, while the BSP component remains constrained by the 2022 GLC_FCS30D layer. These 2023 NDVI and NTL observations are auxiliary to the recent status classification only and do not extend the DEV/REC dataset beyond 2022.

We have revised Section 2.3 to make this temporal distinction explicit and to clarify that the 2023 NDVI and NTL observations are used only for recent polygon-level status classification, not for extending the DEV/REC dataset beyond 2022.

Manuscript revision: Lines 277-287, Section 2.3.

Original text:

To evaluate the recent developmental trajectories (2019-2023) and current status of global surface mining areas, we employed three indicators: NDVI, BSP, and NTL. NDVI was obtained from the MODIS MOD13Q1 and MYD13Q1 (Collection 6.1) products, and annual maximum NDVI composites at 250-m resolution were generated by combining Terra and Aqua observations for each year. The annual maximum value composite approach was adopted to minimize residual cloud contamination and to better represent peak vegetation conditions. BSP was calculated in this study based on the GLC_FCS30D dataset. Nighttime light data were obtained from the VIIRS Day/Night Band monthly product (NOAA, dataset ID: NOAA/VIIRS/DNB/MONTHLY_V1/VCMSLCFG) via Google Earth Engine.

Revised text:

To evaluate the recent developmental trajectories (2019-2023) and current status of global surface mining areas, we employed three indicators: NDVI, BSP, and NTL. NDVI was obtained from the MODIS MOD13Q1 and MYD13Q1 (Collection 6.1) products, and annual maximum NDVI composites at 250-m resolution were generated by combining Terra and Aqua observations for 2019-2023. The annual maximum value composite approach was adopted to minimize residual cloud contamination and to better represent peak vegetation conditions. BSP was calculated in this study based on the GLC_FCS30D dataset for 2019-2022. Nighttime light data were obtained from the VIIRS Day/Night Band monthly product (NOAA, dataset ID: NOAA/VIIRS/DNB/MONTHLY_V1/VCMSLCFG) via Google Earth Engine for 2019-2023.

Response to Report #3 - Anonymous referee #2

Reviewer's Comment: *"The authors have done an excellent job addressing my previous concerns. I have only one remaining comment regarding the dataset: While I understand that the current temporal coverage ending in 2022 is constrained by the availability of the GLC_FCS30D dataset, I remain concerned that the dataset may not be sufficiently up to date. I recommend that the authors consider incorporating complementary or supplementary datasets to extend the temporal coverage and update the existing results accordingly.*
Beyond this point, I have no additional comments."

Response:

We sincerely thank the referee for the positive evaluation of our revision and for this constructive suggestion. We fully agree that keeping the dataset current is important, and we did consider extending the time series beyond 2022 using complementary land-cover products. After surveying the currently available options, we found that no global product matches the 30 m resolution, Landsat-based sensor basis, and class detail of GLC_FCS30D closely enough to be appended without introducing a methodological discontinuity; the cross-product comparison with CLCD that we added in response to Referee #1 further confirms that inferred mining transitions, particularly reclamation, depend non-trivially on the choice of source LULC product. For the present release we therefore kept 2022 as the endpoint to preserve temporal consistency across the 1985–2022 record, and we have added a brief note to the manuscript committing to extend the time series in future releases once an updated GLC_FCS30D layer, or a sufficiently harmonized comparable product, becomes available. We appreciate the referee's suggestion and will prioritise it in future dataset updates.

Manuscript revision:

Location: Lines 1015-1024, Section 4.3.

New text:

The current release covers 1985–2022, the full temporal range of the underlying GLC_FCS30D land-cover product. We evaluated currently available global land-cover products for the possibility of extending the time series beyond 2022, but found that none match the 30 m resolution, Landsat-based sensor basis, and class detail of GLC_FCS30D closely enough to be appended without introducing a methodological discontinuity. The cross-product sensitivity assessment reported earlier in this section further indicates that inferred mining transitions, particularly reclamation, depend non-trivially on the choice of source LULC product. Future releases will extend the time series when updated GLC_FCS30D layers, or a sufficiently harmonized comparable product, become available.

Additional Author Revisions

Revision 1: Colour scheme of Figure A6 (Lines 1078, Appendix A)

Editor's request:

"Please ensure that the colour schemes used in your maps and charts allow readers with colour vision deficiencies to correctly interpret your findings (see e.g. FA6). Please check your figures using the Coblis Color Blindness Simulator (https://www.color-blindness.com/coblis-color-blindness-simulator/) and revise the colour schemes accordingly."

Response:

We thank the editor for this reminder. We checked the colour scheme of Figure A6 and revised it to improve accessibility for readers with colour vision deficiencies. In the updated version, the original green bars and red dashed reference lines were replaced with colourblind-friendly blue bars and black dashed reference lines. This change does not affect the underlying data or interpretation, but improves the readability and accessibility of the figure in accordance with the journal's figure standards.

Figure. A6 Reclamation rate of top 15 countries by mining area, 2022.

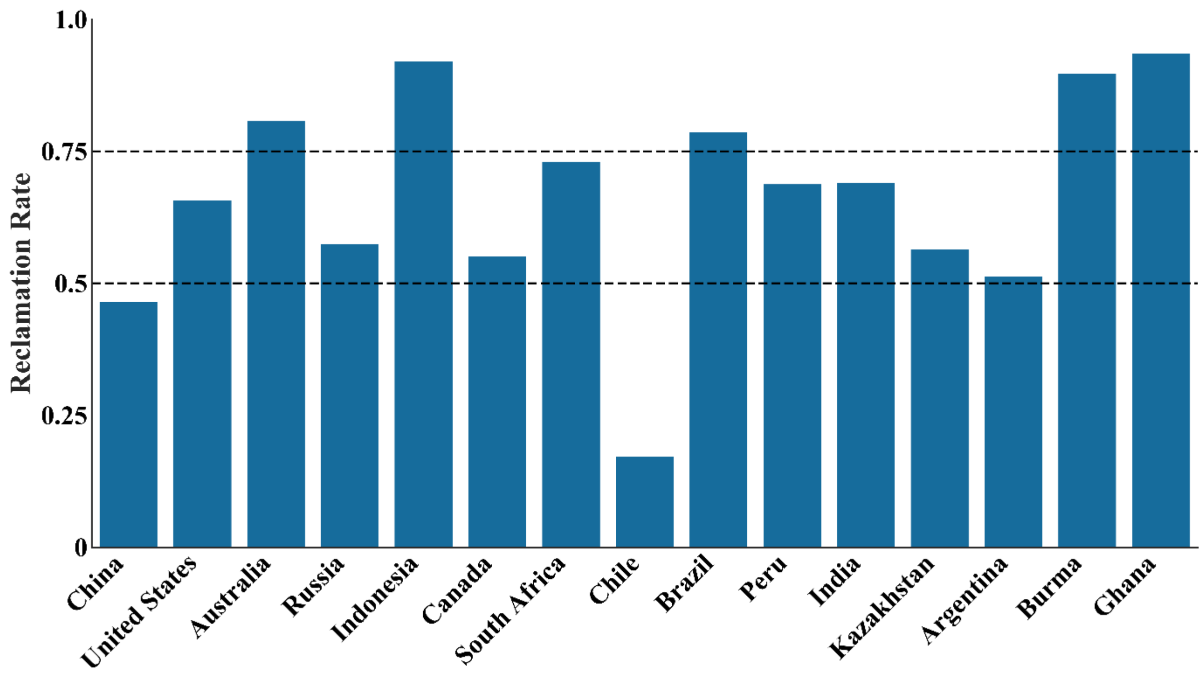

Revision 2: Copyright statement for Figure 3 (Lines 378-379, Section 2.4)

Editor's request:

"Regarding your figure 3: please note that in accordance with our standards, material that originated from Google Earth requires the copyright symbol "©". Please add it to the caption of Figure 3 with the next revision. For instance, © Google Earth Engine or © Google Maps."

Response:

We thank the editor for pointing this out. We have revised the caption of Figure 3 to include the required copyright statement for the background imagery. The caption now specifies: "Background imagery: © Google Earth Engine."

Revision 3: Correction of reclamation-rate statistics and Figure A6

During our final consistency check of the Results section and the supporting figure, we re-examined the calculation of the reclamation-rate statistics and found that the previous text mixed the auxiliary 2023 status-related indicators with the 2022 BSP-based reclamation-rate map. To ensure consistency with the temporal coverage of the mining dataset and Figure 7e, we recalculated the national and global reclamation rates using the 2022 polygon-level BSP results. Specifically, the reclamation rate was calculated as 1 - BSP, and the national and global values were computed as area-weighted averages based on mining polygon area. Accordingly, we revised the Results text and updated Figure A6 using the corrected 2022 area-weighted values for the top 15 countries ranked by mining area. The revised values are more internally consistent with the 2022 BSP map and the final polygon-level statistics. The correction therefore improves numerical consistency without changing the main conclusion that reclamation progress is spatially uneven across major mining countries.

Author's revision: Lines 611-637, Section 3.2.

Revised text:

By 2022, the global average reclamation rate of surface mining land reached 62.6 %. In this study, the reclamation rate was calculated as 1 - BSP, where BSP represents the proportion of mine-related bare surface classes within each mining polygon. National and global values were calculated as area-weighted averages using the mining polygon area. Therefore, this metric should be interpreted as a land-cover-based indicator of reclamation status rather than a direct field measurement of ecological restoration. The spatial pattern shown in Fig. 7e indicates that unreclaimed or actively disturbed mining surfaces remain concentrated in several major mining regions, including northern China, Central Asia, eastern Europe, western North America, the Andes, southern Africa, and parts of Australia. In contrast, many mining regions in Southeast Asia, tropical South America, parts of Africa, and Oceania showed lower proportions of exposed mine-related bare surfaces, suggesting a higher degree of land-cover recovery within mapped mining polygons.

At the national level, the top 15 countries ranked by mapped surface mining area showed substantial differences in reclamation rates (Fig. A6). Among these countries, Ghana (93.7 %) and Indonesia (92.1 %) showed the highest reclamation rates, followed by Australia (80.8 %), Brazil (78.8 %), South Africa (73.1 %), India (69.1 %), Peru (68.9 %), and the United States (65.9 %), all exceeding the global average. In contrast, China (46.6 %), Chile (17.3 %), Canada (55.3 %), Kazakhstan (56.6 %), and Russia (57.5 %) were below the global average, indicating that large surface mining footprints do not necessarily correspond to high reclamation rates. China, which contains the largest number of mapped mining polygons globally, had a reclamation rate substantially below the global average, highlighting the continuing restoration pressure associated with high-intensity mining. Chile showed the lowest reclamation rate among the top 15 countries, consistent with the concentration of large exposed mining surfaces in the Andes.

Author's revision: Lines 973-980, Section 4.3.

Original text:

Finally, the reclamation rate in this study was calculated as 1−BSP, representing the proportion of vegetated cover within mining areas. While this proxy provides a consistent and scalable measure of greening by quantifying the proportion of vegetated cover within mining boundaries, it does not necessarily reflect actual reclamation practices or ecological restoration outcomes. Therefore, the global average reclamation rate of 70.3 % reported for 2023 should be viewed as an indicator of vegetation presence, which likely overestimates the extent of true ecological recovery.

Revised text:

Finally, the reclamation rate in this study was calculated as 1−BSP, where BSP represents the proportion of mine-related bare surface classes within mapped mining polygons. This metric should be interpreted as a land-cover-based reclamation proxy rather than a field-confirmed measure of ecological restoration. Because non-mine-related land-cover classes are not necessarily equivalent to successful ecological restoration, the global average reclamation rate reported for 2022 should be viewed as an indicator of land-cover recovery within mapped mining boundaries rather than a direct measure of completed reclamation practice.

Revision 4: Correction of the spectral-index data source used in temporal validation

During our review of the temporal-validation description, we found that the original manuscript incorrectly stated that the NDVI, NDWI, and NBR indices used in the validation were derived from Sentinel-2 MSI surface reflectance data. This was an inadvertent wording error. The spectral trajectories used for the validation were derived from Landsat Collection 2 Level-2 surface reflectance data from Landsat 4, 5, 7, 8, and 9 over 1985–2024. We corrected the relevant text in Section 2.4 and revised the description to specify the Landsat data source, cloud and saturation masking procedure, and the use of LandTrendr segmentation of annual-maximum NDVI composites. This correction does not change the validation results, but ensures that the data source and validation procedure are accurately described.

Author's revision: Lines 386-399, Section 2.4

Original text:

Reference labels were generated through visual interpretation of high-resolution Google Earth imagery. To enhance the consistency and accuracy of interpretation, LandTrendr-derived segmentation of the annual maximum NDVI time series was integrated, along with complementary spectral profiles from Normalized Difference Water Index (NDWI) and Normalized Burn Ratio (NBR) indices. All three indices (NDVI, NDWI, and NBR) were derived from Sentinel-2 MSI surface reflectance data.

Revised text:

Reference transition years were assigned through visual interpretation of the available high-resolution Google Earth imagery time series, supported by Landsat-based spectral trajectories. Specifically, we used Landsat Collection 2 Level-2 surface reflectance data from Landsat 4, 5, 7, 8, and 9 for the period 1985–2024. Surface reflectance values were scaled using the Collection 2 scale factors, and clouds, cloud shadows, and saturated pixels were masked using the QA_PIXEL and QA_RADSAT bands. For each valid Landsat observation, we calculated NDVI together with complementary Normalized Difference Water Index (NDWI) and Normalized Burn Ratio (NBR) to assist the interpretation of disturbance and recovery signals. Annual maximum NDVI composites were further generated and segmented using the LandTrendr algorithm to identify major breakpoints in the vegetation trajectory. The final reference transition year for each validation sample was determined by jointly considering the high-resolution imagery record, the LandTrendr segmentation result, and the multi-year Landsat spectral-index profiles.

Revision 5: Correction of the text typesetting error

Author’s revision: Lines 359, Section 2.4

Original text： A total of 750 validation points (Fig. A1):were randomly sampled...

Revised text： A total of 750 validation points (Fig. A1) were randomly sampled...

Revision 6: Correction of the proportion of active mines concentrated in Asia (Abstract)

During our final consistency check between the Abstract and Section 3.3, we identified an inconsistency in the reported proportion of active mines concentrated in Asia. The Abstract previously stated "approximately 48.9 % concentrated in Asia", but Section 3.3 (and Fig. 8c) shows that 11,953 active mines in Asia represent 50.6 % of the global active mine count. The 48.9 % figure used in the previous Abstract corresponded instead to the global proportion of undefined mines, and was inadvertently quoted in the Asian active-mine sentence. We have corrected the Abstract figure so that it matches the value reported in Section 3.3.

Author's revision: Lines 35-36, Abstract.

Original text: Active mining areas dominated the global mining landscape, comprising 31.6 % of all polygons, with approximately 48.9 % concentrated in Asia.

Revised text: Active mining areas dominated the global mining landscape, comprising 31.6 % of all polygons, with approximately 50.6 % concentrated in Asia.

Revision 7: Unification of the mining-status classification terminology (undefined → stable)

During our consistency review, we noted that two terms—"undefined mines" and "stable mines"—had been used interchangeably across Section 3.3, Section 4.2 and Section 4.3 to refer to the same classification category. Most occurrences in the manuscript already used "stable"; only the main classification statement at the start of Section 3.3 and the Figure 8 caption still used "undefined". To eliminate ambiguity, we standardised the term to "stable" by replacing the two remaining "undefined" occurrences.

Author's revision: Section 3.3, Lines 654-655, Line 658; Figure 8 caption, Line 692.

Revision 8: Updated validation summary in the study overview

During our consistency review with Section 2.4, we noted that the validation summary at the end of the study-overview paragraph in the Introduction did not yet reflect the three-component validation framework adopted in the revised Section 2.4. We have updated the sentence so that the overview matches the revised methodology (Change #2 in the Summary of All Changes) and so that the cited 67 % accuracy is correctly attributed to the temporal validation across global biomes, rather than read as an overall dataset accuracy.

Author's revision: Lines 144-148, study-overview paragraph at the end of the Introduction.

Original text: The dataset was validated using random stratified sampling, achieving an overall accuracy of 67 %.

Revised text: The dataset was validated through a three-component framework comprising spatial validation against existing global mining datasets, temporal validation of transition years against trajectory-based reference samples, and a cross-product sensitivity assessment using CLCD; the temporal validation achieved an overall accuracy of 67 % across global biomes.

Revision 9: Update of the affiliation of co-first author Sucheng Xu

During the final preparation of this revision, we updated the affiliation of the co-first author Sucheng Xu to additionally include the Institute for Ecological Economics, Vienna University of Economics and Business (WU), Vienna, Austria, reflecting his current research collaboration. The corresponding affiliation labels in the author list have been updated accordingly. No other changes were made to authorship, author order, or contributions.

Author's revision: Line 3, author list.

Original text: Sucheng Xu [a,1], Jiatong Zhou [a,2], Kechao Wang [a], Stefan Giljum [c], Victor Maus [c,d], Tim T. Werner [e], Liang Tang [f], Jiwang Guo [a],Wu Xiao [a,b,*]

Revised text: Sucheng Xu [a,c,2], Jiatong Zhou [a,2], Kechao Wang [a], Stefan Giljum [c], Victor Maus [c,d], Tim T. Werner [e], Liang Tang [f], Jiwang Guo [a],Wu Xiao [a,b,*]

Summary of All Changes

Table R3. Summary of all changes.

No.	Reviewer	Comment	Change Description	Location in Revised Manuscript
1	Referee #1	Comment 1	Clarified that DEV and REC layers are inferred from GLC_FCS30D land-cover transitions within mining boundaries, not from direct spectral-temporal breakpoint detection; consistently relabelled them as "GLC_FCS30D-based land-cover transition products" and clarified that "reclamation" denotes remotely sensed greening rather than field-confirmed restoration.	Section 2.2, Lines 248-254
2	Referee #1	Comment 2	Revised the validation framework from a dual-track design to a three-component framework comprising spatial validation, temporal validation, and a new cross-product sensitivity assessment; updated the workflow figure accordingly.	Section 2.4, Lines 337-347; Figure 1
3	Referee #1	Comment 2	Added a methodological description of the object-based cross-product sensitivity assessment using CLCD (27,948 Chinese mining polygons, 2001–2022), including class equivalence, transition rule, and polygon-level metrics.	Section 2.4, Lines 423-441
4	Referee #1	Comment 2	Added a quantitative discussion of the CLCD vs GLC_FCS30D cross-product comparison results in Section 4.3, reporting cumulative transition area, polygon-level co-detection rates, and mean transition-year offsets to	Section 4.3, Lines 876-901

[1] *These authors contributed equally to this work.*

[*] *Corresponding author: Wu Xiao, xiaowu@zju.edu.cn.*

[2] *These authors contributed equally to this work.*

[*] *Corresponding author: Wu Xiao, xiaowu@zju.edu.cn.*

			bound source-LULC-related uncertainty.	
5	Referee #1	Comment 3	Made the temporal-resolution constraint of GLC_FCS30D explicit: pre-2000 maps are at five-year intervals so transition timing was interpolated, and pre-2000 annual area estimates should be read as interval-averaged values.	Section 2.2, Lines 245-248
6	Referee #1	Comment 4	Addressed by the cross-product sensitivity assessment introduced for Comment 2 (no additional standalone manuscript revision; refers to changes #2–#4).	See changes #2–#4
7	Referee #2	Major Comment 1	Added an explicit scope statement in Section 2.1 noting that the integration step refines and harmonizes known mining footprints but cannot discover mining sites absent from both source inventories.	Section 2.1, Lines 177-182
8	Referee #2	Major Comment 1	Expanded Section 4.3 to acknowledge spatial incompleteness arising from reliance on two static circa-2020 source inventories, and identified three regimes (newly developed mines, small/informal sites, shared omissions) likely to be under-represented.	Section 4.3, Lines 903-919
9	Referee #2	Major Comment 2	Rewrote the temporal-validation description to clarify that the 1,000 samples are stratified by nominal transition year but each pixel is interpreted using the full multi-decadal trajectory; renamed the metric as transition-year accuracy and described the LandTrendr-based reference assignment.	Section 2.4, Lines 381-402
10	Referee #2	Major Comment 2	Added a sample-size limitation statement noting that 1,000 trajectory-interpreted samples remain limited for a global dataset and that future work should expand and further stratify the reference set.	Section 4.3, Lines 1008-1013
11	Referee #2	Major Comment 3	Clarified that the polygon-level NDVI/BSP/NTL indicators are aggregated within each mining polygon to construct polygon-level annual time series for the Mann–Kendall trend test.	Section 2.3, Lines 291-292
12	Referee #2	Major Comment 3	Added a discussion of MODIS NDVI mixed-pixel effects for small or narrow mining polygons, clarified that this affects only the recent status classification (not the 30 m DEV/REC layers), and suggested harmonized Landsat–Sentinel vegetation-index series as a future improvement.	Section 4.3, Lines 951-971
13	Referee #2	Minor Comment 1	Improved Figure 4 readability by enlarging axis-label, tick-label, and legend fonts in the spectral-trajectory panels and adding a clearer annotation for the LCTS mining-year	Figure 4 and caption, Section 2.4

			reference line.	
14	Referee #2	Minor Comment 2	Clarified that the released DEV/REC area and year layers cover 1985–2022, while 2023 NDVI and NTL observations are used only as auxiliary indicators for recent polygon-level status classification (BSP from 2019–2022; MODIS NDVI and VIIRS NTL for 2019–2023).	Section 2.3, Lines 277-287
15	Referee #3	Comment 1	Added a future-update statement explaining that the dataset is currently bounded by the temporal range of GLC_FCS30D and will be extended once an updated GLC_FCS30D layer or a sufficiently harmonized comparable product becomes available.	Section 4.3, Lines 1015-1024
16	Editor request	Add. Rev. 1	Revised the colour scheme of Figure A6 from green bars / red dashed reference lines to colourblind-friendly blue bars / black dashed reference lines, in accordance with the Coblis Color Blindness Simulator check.	Figure A6, Appendix A (caption Line 1078)
17	Editor request	Add. Rev. 2	Added the required copyright statement ("Background imagery: © Google Earth Engine.") to the Figure 3 caption.	Figure 3 caption, Section 2.4, Lines 378-379
18	Author revision	Add. Rev. 3	Recomputed national and global reclamation rates using the 2022 polygon-level BSP (1 - BSP, area-weighted) to remove a previous inconsistency between 2023 status indicators and the 2022 BSP map; updated the Results text and Figure A6 with the corrected 2022 area-weighted top-15 country values.	Section 3.2, Lines 611-637; Figure A6, Appendix A
19	Author revision	Add. Rev. 3	Reworded the limitation discussion of the reclamation rate to make explicit that 1 - BSP is a land-cover-based proxy referenced to 2022, not a field-confirmed restoration measure.	Section 4.3, Lines 973-980
20	Author revision	Add. Rev. 4	Corrected the temporal-validation data source: the spectral indices (NDVI, NDWI, NBR) used for trajectory interpretation were derived from Landsat Collection 2 Level-2 surface reflectance (Landsat 4/5/7/8/9, 1985–2024), not Sentinel-2 MSI; added the QA masking and LandTrendr-segmentation procedure.	Section 2.4, Lines 386-399
21	Author revision	Add. Rev. 5	Corrected a typesetting error in the spatial-validation paragraph by removing an unintended colon after "(Fig. A1)".	Section 2.4, Line 359
22	Author revision	Add. Rev. 6	Corrected the proportion of active mines concentrated in Asia in the Abstract from 48.9 % to 50.6 %, aligning the figure with the	Abstract, Lines 35-36

			value reported in Section 3.3 (11,953 / 23,638 active mines).	
23	Author revision	Add. Rev. 7	Unified the mining-status classification terminology by replacing the two remaining occurrences of "undefined" with "stable" for the 48.9 % category, so that the classification name in the main classification statement and Figure 8 caption matches the wording already used in the subsequent discussion paragraphs of Section 3.3, Section 4.2 and Section 4.3.	Section 3.3, Lines 654-655, Line 658; Figure 8 caption, Line 692
24	Author revision	Add. Rev. 8	Updated the validation summary sentence in the study-overview paragraph (end of Introduction) to reflect the three-component validation framework adopted in the revised Section 2.4 and to correctly attribute the 67 % accuracy to the temporal validation across global biomes.	Introduction, Lines 144-148
25	Author revision	Add. Rev. 9	Updated the affiliation of co-first author Sucheng Xu to additionally include the Institute for Ecological Economics, Vienna University of Economics and Business (WU), Vienna, Austria.	Author list, Line 3

References cited in the response

[1] Zhang, X., Zhao, T., Xu, H., Liu, W., Wang, J., Chen, X., and Liu, L., 2024. GLC_FCS30D: the first global 30 m land-cover dynamics monitoring product with a fine classification system for the period from 1985 to 2022 generated using dense-time-series Landsat imagery and the continuous change-detection method. Earth System Science Data, 16(3), 1353–1381. https://doi.org/10.5194/essd-16-1353-2024

[2] Zanaga, D., Van De Kerchove, R., De Keersmaecker, W., Souverijns, N., Brockmann, C., Quast, R., Wevers, J., Grosu, A., Paccini, A., Vergnaud, S., Cartus, O., Santoro, M., Fritz, S., Georgieva, I., Lesiv, M., Carter, S., Herold, M., Li, L., Tsendbazar, N.-E., Ramoino, F., and Arino, O., 2021. ESA WorldCover 10 m 2020 v100. Zenodo. https://doi.org/10.5281/zenodo.5571936

[3] Zanaga, D., Van De Kerchove, R., Daems, D., De Keersmaecker, W., Brockmann, C., Kirches, G., Wevers, J., Cartus, O., Santoro, M., Fritz, S., Lesiv, M., Herold, M., Tsendbazar, N.-E., Xu, P., Ramoino, F., and Arino, O., 2022. ESA WorldCover 10 m 2021 v200. Zenodo. https://doi.org/10.5281/zenodo.7254221

[4] Defourny, P., Lamarche, C., Bontemps, S., De Maet, T., Van Bogaert, E., Moreau, I., Brockmann, C., Boettcher, M., Kirches, G., Wevers, J., Santoro, M., Ramoino, F., and Arino,

O., 2022. Land Cover Classification Gridded Maps from 1992 to Present Derived from Satellite Observations. Copernicus Climate Change Service (C3S) Climate Data Store. https://doi.org/10.24381/cds.006f2c9a

[5] Friedl, M. and Sulla-Menashe, D., 2022. MODIS/Terra+Aqua Land Cover Type Yearly L3 Global 500 m SIN Grid V061 [Data set]. NASA EOSDIS Land Processes Distributed Active Archive Center. https://doi.org/10.5067/MODIS/MCD12Q1.061

[6] Chen, J., Chen, J., Liao, A., Cao, X., Chen, L., Chen, X., He, C., Han, G., Peng, S., Lu, M., Zhang, W., Tong, X., and Mills, J., 2015. Global land cover mapping at 30 m resolution: A POK-based operational approach. ISPRS Journal of Photogrammetry and Remote Sensing, 103, 7–27. https://doi.org/10.1016/j.isprsjprs.2014.09.002

[7] Buchhorn, M., Lesiv, M., Tsendbazar, N.-E., Herold, M., Bertels, L., and Smets, B., 2020. Copernicus Global Land Cover Layers—Collection 2. Remote Sensing, 12(6), 1044. https://doi.org/10.3390/rs12061044

[8] Brown, C. F., Brumby, S. P., Guzder-Williams, B., Birch, T., Hyde, S. B., Mazzariello, J., Czerwinski, W., Pasquarella, V. J., Haertel, R., Ilyushchenko, S., Schwehr, K., Weisse, M., Stolle, F., Hanson, C., Guinan, O., Moore, R., and Tait, A. M., 2022. Dynamic World, Near real-time global 10 m land use land cover mapping. Scientific Data, 9, 251. https://doi.org/10.1038/s41597-022-01307-4

[9] Yang, J. and Huang, X., 2021. The 30 m annual land cover dataset and its dynamics in China from 1990 to 2019. Earth System Science Data, 13(8), 3907–3925. https://doi.org/10.5194/essd-13-3907-2021

Added References in Manuscript

[1] Yang, J. and Huang, X., 2021. The 30 m annual land cover dataset and its dynamics in China from 1990 to 2019. Earth System Science Data, 13(8), 3907–3925. https://doi.org/10.5194/essd-13-3907-2021

We believe that these revisions have substantially strengthened the manuscript and adequately addressed all concerns raised by the reviewers. We are grateful for the constructive feedback and remain open to further suggestions.

Sincerely,
The Authors